

# On the Use of Spherical, Ellipsoidal and Prismatic Hulls to Predict Equivalent Stress Ranges in Multiaxial Fatigue

*Marco Antonio Meggiolaro, Jaime Tupiassú Pinho de Castro*

Pontifical Catholic University of Rio de Janeiro - Dept. of Mechanical Engineering  
Rua Marquês de São Vicente 225, Gávea – Rio de Janeiro, RJ Brazil 2453-900

Non-proportional (NP) multiaxial fatigue life predictions require the calculation of equivalent stress or strain ranges associated with the history path. A traditional way to find such ranges is to use spherical, ellipsoidal or prismatic hull methods, which search for enclosures of the entire history path in stress or strain diagrams. In this work, all existing hull methods are presented and compared using results from more than 3,000,000 Monte Carlo simulations of random and especially chosen path topologies in stress or strain diagrams. New models are also proposed, based on Deperrois' idea of longest chords. It is found that the proposed models are very similar to the Maximum Prismatic Hull model, but with a much simpler and efficient algorithm to compute equivalent stresses. It is also shown that the Minimum Circumscribed Ellipsoid, Minimum Volume Ellipsoid, and Minimum Ball methods may result in very poor predictions of the stress or strain amplitudes. The only recommended method based on ellipsoids is the Minimum F-norm Ellipsoid which, together with the Maximum Prismatic Hull model and its variations, is efficient to predict equivalent amplitudes in NP histories.

Keywords: multiaxial fatigue; equivalent stress; convex hull

## 1. Introduction

Multiaxial fatigue damage models are based on stress or strain ranges. It is not difficult to define these ranges for constant amplitude loadings, where only two stress or strain states need to be considered, one associated with the peak and the other with the valley. However, for multiaxial variable amplitude (VA) loadings, in special when the history is non-proportional (NP), it is not clear how these ranges should be defined and identified.

Consider that the periodic history is formed by repeatedly following a given loading path domain  $D$ , where  $D$  contains all points from the stress or strain variations along one period of the history. For a complex-shaped history, it is not easy to decide how to obtain the effective maximum strain range  $\Delta\tau_{max}$  associated with  $D$ . The so-called convex hull methods [1-5] try to find circles, ellipses or rectangles that contain the entire path (in the 2D case). In a nutshell, in the 2D case, the Minimum Ball (MB) method [1] searches for the circle with minimum radius that contains  $D$ ; the minimum ellipse methods [2-4] search for an ellipse with semi-axes  $a$  and  $b$  that contains  $D$  with minimum area  $\pi a \cdot b$  or minimum norm  $(a^2 + b^2)^{1/2}$ ; and the maximum prismatic hull methods [3, 5] search among the smallest rectangles that contain  $D$  the one with maximum area or maximum diagonal (it's a max-min search problem). The value of  $\Delta\tau_{max}$  in Fig. 1 would either be assumed as the value of the circle diameter, or twice the ellipse norm, or the rectangle diagonal. If the history path were represented in a shear strain  $\gamma_B \times$  shear strain  $\gamma_{B2}$  diagram, these exact same methods would result in estimates for the effective maximum shear strain range  $\Delta\gamma_{max}$ .

The convex hull methods can also be applied to traction-torsion histories, if a  $\sigma_x \times \tau_{xy} \sqrt{3}$  diagram is considered. The effective range in this case is the Mises stress range  $\Delta\sigma_{Mises}$ . Similarly, for traction-torsion histories where plastic strains dominate, a strain diagram  $\varepsilon_x \times \gamma_{xy} \sqrt{3}$  can be used to predict an effective Mises strain range  $\Delta\varepsilon_{Mises}$ .

Such convex hull methods can be extended to histories involving more than two stress or strain components. E.g., if the history path is plotted in a 3D diagram representing 3 stress or strain components, the convex hull methods will search for spheres, ellipsoids or rectangular prisms. For higher dimension diagrams, the search is for hyperspheres, hyperellipsoids, and rectangular hyperprisms.

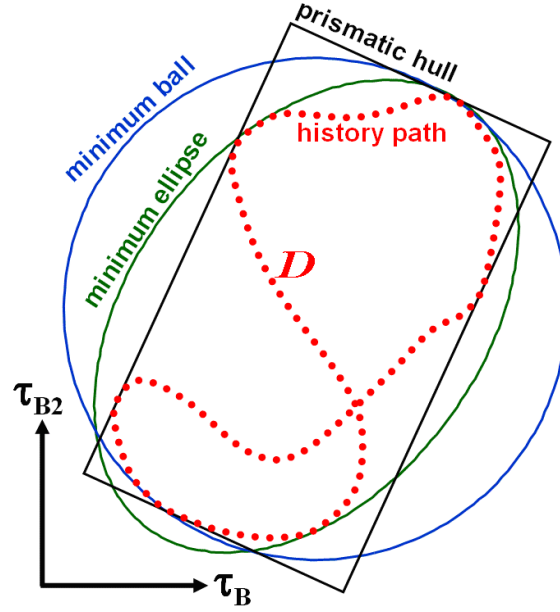


Fig. 1: Stress history path  $D$  in a shear stress  $\tau_B \times$  shear stress  $\tau_{B2}$  diagram, enclosed in convex hulls based on circles (balls), ellipses and rectangular prisms.

The convex hull methods are described in detail in the following sections. Their framework is based on deviatoric stress (or strain) diagrams and Mises stress (or strain) parameters, which are discussed next.

## 2. Mises Stress and Strain Parameters

The methods to obtain effective (or equivalent) stress and strain ranges usually make use of stress and strain parameters based on the Mises yield function. For linear elastic histories, both Mises effective stress  $\sigma_{Mises}$  and Mises (or octahedral) shear stress  $\tau_{Mises}$  can be used as auxiliary parameters, where

$$\sigma_{Mises} = \frac{3}{\sqrt{2}} \tau_{Mises} = \frac{1}{\sqrt{2}} \sqrt{(\sigma_x - \sigma_y)^2 + (\sigma_y - \sigma_z)^2 + (\sigma_x - \sigma_z)^2 + 6(\tau_{xy}^2 + \tau_{yz}^2 + \tau_{xz}^2)} \quad (1)$$

Since the Mises stress  $\sigma_{Mises}$  (as well as the octahedral shear stress  $\tau_{Mises}$ ) equation is always positive, a Mises stress range  $\Delta\sigma_{Mises}$  (also known as relative Mises stress  $\sigma_{RMises}$ ) should be used to correctly evaluate the variation of  $\sigma_{Mises}$  due to a change  $(\Delta\sigma_x, \Delta\sigma_y, \Delta\sigma_z, \Delta\tau_{xy}, \Delta\tau_{xz}, \Delta\tau_{yz})$  in the stress components along some loading path  $\Delta$ :

$$\Delta\sigma_{Mises} = \sigma_{RMises} = \frac{\sqrt{(\Delta\sigma_x - \Delta\sigma_y)^2 + (\Delta\sigma_x - \Delta\sigma_z)^2 + (\Delta\sigma_y - \Delta\sigma_z)^2 + 6(\Delta\tau_{xy}^2 + \Delta\tau_{xz}^2 + \Delta\tau_{yz}^2)}}{\sqrt{2}} \quad (2)$$

Note that the Mises stress range correlates with the octahedral shear range parameter  $\Delta\tau_{Mises}$ , used in both Sines and Crossland models, through  $\Delta\sigma_{Mises} = \Delta\tau_{Mises} \cdot 3/\sqrt{2}$ .

The Mises effective strain  $\varepsilon_{Mises}$  is another useful quantity in VA-NP histories, in special to deal with plastic strains. It uses the mean or effective Poisson coefficient  $\bar{\nu} = (0.5\varepsilon_{pl} + \nu_{el}\varepsilon_{el}) / (\varepsilon_{pl} + \varepsilon_{el})$  to include plastic effects, where  $\varepsilon_{el}$  and  $\varepsilon_{pl}$  are the elastic and plastic components of the strains, and  $\nu_{el}$  and  $\nu_{pl}$  are the elastic and plastic Poisson coefficients (where  $\nu_{pl} = 0.5$ ). The Mises strain correlates with the octahedral (or Mises) shear strain  $\gamma_{Mises}$ , which is the combination of both shear strains that act in each of the octahedral planes, through

$$\varepsilon_{Mises} = \frac{3}{2\sqrt{2} \cdot (1 + \bar{\nu})} \gamma_{Mises} = \frac{\sqrt{(\varepsilon_x - \varepsilon_y)^2 + (\varepsilon_x - \varepsilon_z)^2 + (\varepsilon_y - \varepsilon_z)^2 + 1.5(\gamma_{xy}^2 + \gamma_{xz}^2 + \gamma_{yz}^2)}}{\sqrt{2} \cdot (1 + \bar{\nu})} \quad (3)$$

Since the  $\varepsilon_{Mises}$  (as well as the  $\gamma_{Mises}$ ) equation is always positive, a Mises strain range  $\Delta\varepsilon_{Mises}$  (also known as the relative Mises strain  $\varepsilon_{RMises}$ ) should be used to evaluate its variation due to a change ( $\Delta\varepsilon_x$ ,  $\Delta\varepsilon_y$ ,  $\Delta\varepsilon_z$ ,  $\Delta\gamma_{xy}$ ,  $\Delta\gamma_{xz}$ ,  $\Delta\gamma_{yz}$ ) in the strain components along some loading path:

$$\Delta\varepsilon_{Mises} = \varepsilon_{RMises} = \frac{\sqrt{(\Delta\varepsilon_x - \Delta\varepsilon_y)^2 + (\Delta\varepsilon_x - \Delta\varepsilon_z)^2 + (\Delta\varepsilon_y - \Delta\varepsilon_z)^2 + 1.5(\Delta\gamma_{xy}^2 + \Delta\gamma_{xz}^2 + \Delta\gamma_{yz}^2)}}{\sqrt{2} \cdot (1 + \bar{\nu})} \quad (4)$$

An octahedral (or Mises) shear range parameter  $\Delta\gamma_{Mises}$  can also be defined, related to the Mises strain range by

$$\Delta\varepsilon_{Mises} = \frac{3 \cdot \Delta\gamma_{Mises}}{2\sqrt{2}(1 + \bar{\nu})} \quad (5)$$

Note that the octahedral stress or strain shear ranges  $\Delta\tau_{Mises}$  or  $\Delta\gamma_{Mises}$  are measured on the octahedral planes, they are not equal to twice the shear amplitudes  $\tau_a$  or  $\gamma_a$  acting on the considered plane. But those shear amplitudes could be easily obtained by

$$\tau_a = \frac{\sqrt{6}}{4} \Delta\tau_{Mises} = \frac{\sqrt{3}}{6} \Delta\sigma_{Mises} \quad \text{and} \quad \gamma_a = \frac{\sqrt{3}}{6} \Delta\gamma_{Mises} = \frac{1 + \bar{\nu}}{\sqrt{3}} \Delta\varepsilon_{Mises} \quad (6)$$

Finally, for the linear elastic case, all these relative Mises stresses and strains correlate with the Mises shear range parameters by

$$\Delta\sigma_{Mises} = E \cdot \Delta\varepsilon_{Mises} = \frac{3}{\sqrt{2}} \cdot \Delta\tau_{Mises} = \frac{3E}{2\sqrt{2} \cdot (1 + \bar{\nu})} \cdot \Delta\gamma_{Mises} \quad (7)$$

### 3. Reduced Order Stress and Strain Spaces

When dealing with incremental plasticity, it is convenient to represent the stresses or strains in a 9-dimensional (9D) space. In particular, when representing the deviatoric stress tensor in 9D, its norm  $|\bar{S}|$  becomes directly proportional to the Mises stress and octahedral (or Mises) shear stress, namely  $|\bar{S}| = \sigma_{Mises} \cdot \sqrt{6}/3 = \tau_{Mises} \cdot \sqrt{3}$ . In addition, the Prandtl-Reuss flow rule results in slightly different (and probably better) equations when formulated in 9D space than the equations derived using a reduced 6-dimensional (6D) formulation.

But, to find effective ranges in VA-NP histories, it is a good idea to work in a space with reduced dimensions, saving computational effort without modifying the results. The reduction from 9D to 6D deviatoric stresses is simply a matter of eliminating the  $\tau_{yx}$ ,  $\tau_{zx}$  and  $\tau_{zy}$  components from the deviatoric stress tensor, which are redundant because  $\tau_{yx} \equiv \tau_{xy}$ ,  $\tau_{zx} \equiv \tau_{xz}$ , and  $\tau_{zy} \equiv \tau_{yz}$ .

Since the deviatoric stresses  $S_x$ ,  $S_y$  and  $S_z$  are linear-dependent, because  $S_x + S_y + S_z = 0$ , it is possible to further reduce the deviatoric stress dimension from 6D to 5D. There are infinite ways to do this, for example replacing the stresses  $S_x$ ,  $S_y$  and  $S_z$  by new variables  $S_1 \equiv a_{x1} \cdot S_x + a_{y1} \cdot S_y + a_{z1} \cdot S_z$  and  $S_2 \equiv a_{x2} \cdot S_x + a_{y2} \cdot S_y + a_{z2} \cdot S_z$ , where the user-defined coefficients  $a_{x1}$ ,  $a_{y1}$ ,  $a_{z1}$ ,  $a_{x2}$ ,  $a_{y2}$  and  $a_{z2}$  are any values that make the vectors  $[a_{x1} \ a_{y1} \ a_{z1}]^T$ ,  $[a_{x2} \ a_{y2} \ a_{z2}]^T$ , and  $[1 \ 1 \ 1]^T$  become linear independent. A notable example of such transformation is the one proposed by Papadopoulos et al. [6], who chose  $[a_{x1} \ a_{y1} \ a_{z1}]^T = [\sqrt{3}/2 \ 0 \ 0]^T$  and  $[a_{x2} \ a_{y2} \ a_{z2}]^T = [0 \ 0.5 \ -0.5]^T$ , resulting in a reduced-order deviatoric stress tensor  $\bar{S}'$  represented in a 5D transformed Euclidean stress-space  $E_{5\sigma}$ , where

$$\begin{cases} \bar{S}' \equiv [S_1 \ S_2 \ S_3 \ S_4 \ S_5]^T \\ S_1 \equiv \sigma_x - \frac{\sigma_y}{2} - \frac{\sigma_z}{2} = \frac{3}{2} S_x, \quad S_2 \equiv \frac{\sigma_y - \sigma_z}{2} \sqrt{3} = \frac{S_y - S_z}{2} \sqrt{3} \\ S_3 \equiv \tau_{xy} \sqrt{3}, \quad S_4 \equiv \tau_{xz} \sqrt{3}, \quad S_5 \equiv \tau_{yz} \sqrt{3} \end{cases} \quad (8)$$

The above defined 5D deviatoric stress  $\bar{S}'$  has three very interesting properties:

- 1) The norm of the 5D vector  $\bar{S}'$  from the  $E_{5\sigma}$  transformed deviatoric stress-space is equal to the Mises equivalent stress  $\sigma_{Mises}$

2) The Euclidean distance in the 5D  $E_{5\sigma}$  stress-space between any 2 points  $\bar{S}'_A = [S_{1A} S_{2A} S_{3A} S_{4A} S_{5A}]^T$  and  $\bar{S}'_B = [S_{1B} S_{2B} S_{3B} S_{4B} S_{5B}]^T$ , respectively associated with the 9D deviatoric stresses  $\bar{S}_A$  and  $\bar{S}_B$ , is equal to the Mises stress range  $\Delta\sigma_{Mises}$  between these stress states

3) The locus of the points which have the same  $\Delta\sigma_{Mises}$  with respect to a point  $\bar{S}'$  in the  $E_{5\sigma}$  deviatoric stress-space is the surface of a hypersphere with center in  $\bar{S}'$  and radius  $\Delta\sigma_{Mises}$ . This is a simple corollary from the second property.

Note that, for unnotched specimens under histories combining uniaxial tension  $\sigma_x$  and torsion  $\tau_{xy}$ , the 5D deviatoric stress  $\bar{S}'$  can be represented in the classical diagram  $\sigma_x \times \tau_{xy} \sqrt{3}$  using the 2D projection  $[S_1 S_3]^T$ , since in this case  $S_1 = \sigma_x$ ,  $S_3 = \tau_{xy} \sqrt{3}$ , and  $S_2 = S_4 = S_5 = 0$ .

After defining all involved stress and strain parameters, the convex hull methods are discussed. These methods are based on convex hulls enclosing the history path in the above defined stress or strain sub-spaces. There are 3 types of convex hulls: balls, ellipsoids and rectangular prisms. The Minimum Ball method is presented next.

#### 4. Minimum Ball Method

Dang Van [1] realized that the search for an effective stress range must take place on the deviatoric stress space. For periodic elastic histories, the mesoscopic stresses and strains in the critically oriented grain should stabilize by the process of elastic shakedown, generating a local residual stress  $[\sigma_{ij}]_{res}$  at such critical grain. Dang Van assumed that the subsequent mesoscopic ( $\mu$ ) stress history at such grain, after the stabilization, is related to the macroscopic ( $M$ ) history through

$$[\sigma_{ij}(t)]_{\mu} = [\sigma_{ij}(t)]_M + dev[\sigma_{ij}]_{res} \quad (9)$$

where  $dev[\sigma_{ij}]_{res}$  is the deviatoric part of the residual stresses tensor stabilized in that grain.

The calculation of the mesoscopic stresses in Dang Van's model can be interpreted as a hardening problem, caused by elastic shakedown. When the periodic macroscopic history is represented in the deviatoric space, Dang Van assumes that the stabilized residual stress is the vector from the center of the minimum ball that circumscribes the history to the origin of the diagram. The word "ball" is used here to describe a circle, sphere or hypersphere, respectively for 2D, 3D or higher dimension histories. The same result holds if the reduced stress  $E_{5\sigma}$  space is used, or a sub-space from it.

The values of the mesoscopic Tresca stress  $\tau_{\mu}(t)$  and mesoscopic hydrostatic stress  $\sigma_{\mu h}(t)$  (which is equal to the macroscopic hydrostatic stress) are calculated for each point in the mesoscopic history path  $D_{\mu}$ . Dang Van then predicts infinite life if and only if all points satisfy the inequality

$$\tau_{\mu}(t) + \alpha_{DV} \cdot \sigma_{\mu h}(t) \leq \beta_{DV} \quad (10)$$

In summary, Dang Van is a type of Minimum Ball (MB) method where each stress state along the history path is compared to a limiting stress level to predict infinite life. However, it is not useful to calculate finite fatigue lives, since it does not deal with stress (or strain) ranges, only with individual stress states.

But the same MB circumscribed to the macroscopic history can be used to estimate an effective Mises stress range  $\Delta\sigma_{Mises}$  (or strain range  $\Delta\varepsilon_{Mises}$ ). The diameter  $d$  of such MB in the transformed deviatoric stress-space  $E_{5\sigma}$  or strain-space  $E_{5\varepsilon}$  (or in a 2D, 3D or 4D sub-space of such spaces) is the magnitude of the variation  $\Delta\bar{S}'$  (or the deviatoric strain variation  $\Delta\bar{\varepsilon}'$ ), which is equal to  $\Delta\sigma_{Mises}$  (or  $\Delta\varepsilon_{Mises}$ ). Therefore, the effective shear ranges  $\Delta\tau_{max}$  (used in the Findley and McDiarmid models) and  $\Delta\gamma_{max}$  (used in the Brown-Miller and Fatemi-Socie models), Mises ranges  $\Delta\sigma_{Mises}$  and  $\Delta\varepsilon_{Mises}$ , and octahedral shear ranges  $\Delta\tau_{Mises}$  (used in the Sines and Crossland models) and  $\Delta\gamma_{Mises}$ , can all be estimated from  $d$  using the MB method by

$$\begin{aligned} \Delta\sigma_{Mises} &= 3 \cdot \Delta\tau_{Mises} / \sqrt{2} = \Delta\tau_{max} \sqrt{3} = (2\tau_a) \cdot \sqrt{3} = |\Delta\bar{S}'| = d \equiv L \cdot \lambda_{MB} \quad \text{or} \\ \Delta\varepsilon_{Mises} &= 3 \cdot \frac{\Delta\gamma_{Mises}}{2\sqrt{2}(1+\bar{\nu})} = \frac{\Delta\gamma_{max} \sqrt{3}}{2(1+\bar{\nu})} = \frac{(2\gamma_a) \cdot \sqrt{3}}{2(1+\bar{\nu})} = |\Delta\bar{\varepsilon}'| = d \equiv L \cdot \lambda_{MB} \end{aligned} \quad (11)$$

where  $L$  is the longest chord in the history (the maximum Euclidean distance in the transformed space between any two points along the history path, measured in either stress or strain units) and  $\lambda_{MB}$  is a dimensionless parameter defined as the ratio between the Mises stress or strain range and  $L$ .

In the 2D case, if any two points from the history define the diameter of a circle that contains the entire path, then their distance  $L$  is equal to the diameter  $d$ , therefore  $\lambda_{MB} = 1.0$ . A notable 2D case is for a path forming an equilateral triangle, where  $\lambda_{MB} = 2/\sqrt{3} \cong 1.155$ . For any other 2D path, it is found that  $1.0 \leq \lambda_{MB} \leq 1.155$ .

## 5. Minimum Ellipsoid Methods

The Minimum Ball (MB) method is not efficient to represent the behavior of NP histories. For instance, it would predict the same Mises ranges for a NP 90° out-of-phase circular path and a proportional path defined by a diameter of this circle, both resulting in  $\lambda_{MB} = 1.0$ . But a higher value of  $\lambda_{MB}$  would certainly be expected for the NP history.

To solve this problem, Freitas et al. [2] proposed the Minimum Circumscribed Ellipsoid (MCE) method. It searches for an ellipse (or ellipsoid or hyperellipsoid, for higher dimensions) that circumscribes the entire history, with its longest semi-axis  $a_1$  equal to the radius of the minimum ball, and with the smallest possible values for the remaining semi-axes  $a_i$  ( $i > 1$ ). The Mises ranges are

$$\Delta\sigma_{Mises} \text{ or } \Delta\varepsilon_{Mises} = 2 \cdot \sqrt{\sum_{i=1}^{dim} a_i^2} \cong 2 \cdot F \quad (12)$$

where  $dim$  is the dimension of the history path,  $2 \leq dim \leq 5$ , and  $F$  is defined as the Frobenius norm of the ellipsoid, which is equal to the square root of the sum of the squares of the ellipsoid semi-axes. Here, the Frobenius norm is essentially an Euclidean distance (or Euclidean norm) between the origin and a point with coordinates  $(a_1, a_2, \dots, a_{dim})$ , since the axes of the reduced stress (or strain) space are orthonormal. In the case of tensors, the Euclidean norm is commonly called the Frobenius norm, usually abbreviated as F-norm.

The ratio  $\lambda_{MCE}$  between the Mises ranges calculated by the MCE method and the longest chord  $L$  reproduces experimental data better than  $\lambda_{MB}$  generated by the MB method. In the 2D case, a NP circular path would result in  $\lambda_{MCE} = \sqrt{2}$  instead of the proportional value  $1.0$ , which is much more reasonable than the Minimum Ball prediction. It is also found that any 2D path results in  $1.0 \leq \lambda_{MCE} \leq \sqrt{2}$ , with the maximum value occurring e.g. for circular and square paths. In general, for any dimension  $dim$ , it is found that  $1.0 \leq \lambda_{MCE} \leq \sqrt{dim}$ , with the maximum value  $\sqrt{dim}$  occurring e.g. for paths that follow the edges of hypercubes or large portions of the surface of hyperspheres.

The downside of the MCE method is the requirement that the longest semi-axis must be equal to the radius of the Minimum Ball. For the rectangular path shown in Fig. 4, this requirement results in a circle as the minimum circumscribed ellipse, with  $\lambda_{MCE} = \sqrt{2} \cong 1.414$ . But this would be true even for very elongated rectangles with very low aspect ratios between their side lengths. The MCE would thus predict  $\lambda_{MCE} = \sqrt{2}$  for an almost proportional rectangular path, instead of the expected value of  $1.0$ .

A possible alternative to the MCE method is to search for the Minimum Volume Ellipsoid (MVE), also known as the Löwner-John Ellipsoid. In the 2D case, it is basically the search for an enclosing ellipse with minimum area. Such MVE method solves the issue with rectangular paths, however it tends to find ellipses with lower aspect ratios than expected. In addition, the search for such ellipsoid or hyperellipsoid can be computationally intensive for 3D or higher dimension histories.

Another alternative to the MCE method is the search for the Minimum F-norm Ellipsoid (MFE) [3]. Instead of searching for the minimum volume (or area), the MFE looks for the ellipse, ellipsoid, or hyperellipsoid with minimum value of its F-norm  $F$ , defined in Eq. (12). Zouain et al. [4] present an efficient (although computationally intensive) method to numerically find such MFE. Other efficient algorithms can be found in [7].

The ratios between the Mises stress or strain ranges  $2 \cdot F$ , calculated from the MCE, MVE and MFE methods, and the longest chord  $L$  are defined, respectively, as  $\lambda_{MCE}$ ,  $\lambda_{MVE}$  and  $\lambda_{MFE}$ . All these ratios must be greater than or equal to  $1.0$ . In the 2D case, a notable path is the one with the shape of an

equilateral triangle with sides  $L$  (which are also its longest chords), where the resulting hull is a circle with diameter  $d = 2L/\sqrt{3}$  and F-norm  $F = d\sqrt{2}$ , resulting in  $\lambda_{MCE} = \lambda_{MVE} = \lambda_{MFE} = 2 \cdot F/L = 2\sqrt{2}/\sqrt{3} \approx 1.633$ . For any other 2D path, it is found that  $1.0 \leq \lambda_{MCE} \leq 1.633$  and  $1.0 \leq \lambda_{MFE} \leq 1.633$ , however  $\lambda_{MVE}$  can reach values beyond 2.0 when a very elongated enclosing ellipse is the solution with minimum area, an indication that the MVE method can be very conservative.

## 6. Maximum Prismatic Hull Methods

Another class of convex hull methods tries to find a rectangular prism with sides  $2a_1, \dots, 2a_{dim}$  that encloses a load history path, where  $dim$  is the dimension of the considered space. There are essentially 4 methods to fit rectangular prisms to the history path.

The first is the Maximum Prismatic Hull (MPH). This method searches for the smallest rectangular prism that encloses the history (the minimum prism), for each possible orientation of the prism. Among them, the one with highest F-norm is chosen. The F-norm and resulting Mises ranges are the same defined in Eq. (12), except that here  $a_i$  are the semi-lengths (half the length) of the sides of the rectangular prism. The MPH was originally proposed by Gonçalves et al. in [3] for sinusoidal time histories, and later extended by Mamiya et al. in [5] for a general NP loading.

Another prismatic hull method is the Maximum Volume Prismatic Hull (MVPH), which searches among the minimum prisms the one with maximum volume. Although the search is for a maximum volume, the F-norm is also used to compute the Mises range. In the 2D case, the MVPH method is essentially the search, among the minimum rectangles that enclose the entire path, of the one with maximum area (it's a max-min problem).

A third method is proposed here, called the Maximum Prismatic Hull with Longest Chords (MPHLC). It is basically an improvement of Deperrois' method [8]. In the Deperrois method, the longest chord  $L_5$  between any two points of the path in the projected 5D deviatoric stress-space  $E_{5\sigma}$  (or deviatoric strain-space  $E_{5\epsilon}$ , for strain histories) is determined. Then, the path is projected onto a 4D stress-subspace  $E_{4\sigma}$  orthogonal to  $L_5$ , and the new longest chord  $L_4$  is computed in this subspace. The path is then projected onto a stress-subspace  $E_{3\sigma}$  orthogonal to both  $L_5$  and  $L_4$ , and the new longest chord  $L_3$  is computed in this subspace. Analogously, the longest chord  $L_2$  is found in the stress-subspace  $E_{2\sigma}$  orthogonal to  $L_5, L_4$  and  $L_3$ . Finally, the longest chord  $L_1$  is found in the stress-subspace  $E_{1\sigma}$  orthogonal to  $L_5, L_4, L_3$  and  $L_2$ .

The Deperrois method provides satisfactory results [9]. However, Papadopoulos [6] criticizes it because, if any longest chord is non-unique, then different rectangular prisms and resulting shear amplitudes could be obtained for the same history. But this non-uniqueness could be easily solved by stating that, when the longest chords are non-unique, then the chosen prismatic hull would be the one with maximum F-norm among all possible results. The use of rectangular prisms with maximum F-norm has shown good results in the MPH method, therefore this could be the solution to Papadopoulos' criticisms.

The combination of the MPH and Deperrois' methods thus leads to the MPHLC method, performed in 4 steps:

- 1) define the longest side  $2a_1$  of the rectangular prism in the direction of the longest chord  $L$  of the history;
- 2) project the history into the sub-space orthogonal to the directions of all sides of the prisms that have already been defined (for a history with dimension  $dim$ , if  $m$  sides have already been chosen, then such sub-space will have  $dim-m$  dimensions);
- 3) define the next side  $2a_i$  of the rectangular prism in the direction of the longest chord measured in the projected sub-space, and repeat step 2 until all sides are found;
- 4) if multiple solutions for the rectangular prism are found, the one with maximum F-norm is chosen – this step addresses Papadopoulos' criticisms [6].

The advantage of the MPHLC method over the MPH or MVPH is that it does not require a numerical search for the prismatic hull orientation. Its orientation is deterministically defined by the longest chords. In special for 3D or higher dimension histories, the MPHLC method can lead to a huge decrease in computational effort. For instance, the orientation of a 5D hyperprism is given by 10 an-

gles, therefore the search for the orientation associated with maximum F-norm (or maximum volume) involves a search in a 10-dimensional space, which can be very costly. In addition, the next sections will show that the MPHLC predictions give almost the same results as the MPH and MVPH methods.

A variation of the MPHLC is also proposed, called the Maximum Prismatic Hull with Container Chords (MPHCC). It is similar to the MPHLC, but all chords that contain the orthogonal projection of the entire history onto them (called here “container chords”) are considered as candidate directions for the sides of the rectangular prism. Note that every longest chord LC is a “container chord” CC, but not every CC is a LC. From the probable multiple solutions for the resulting rectangular prisms, the one with maximum F-norm is chosen.

The ratios between the Mises stress or strain ranges  $2 \cdot F$ , calculated from the MPH, MVPH, MPHLC and MPHCC methods, and the longest chord  $L$  are defined, respectively, as  $\lambda_{MPH}$ ,  $\lambda_{MVPH}$ ,  $\lambda_{MPHLC}$  and  $\lambda_{MPHCC}$ . All these four ratios are, in average, very close to each other, therefore any of the four variations of the prismatic hull methods could be used interchangeably. For a history path with dimension  $dim$ , it is found that  $1 \leq \lambda_{MPHLC} \leq \lambda_{MPHCC} \leq \lambda_{MPH} \leq \sqrt{dim}$ , therefore the MPHCC results in Mises ratios slightly closer to the MPH predictions than the MPHLC. In addition, it is also found that  $1 \leq \lambda_{MVPH} \leq \lambda_{MPH} \leq \sqrt{dim}$ .

In the next section, all convex hull methods presented in this paper are evaluated and compared.

## 7. Comparison among the Convex Hull Methods

To compare all convex hull methods, it is necessary to study all possible history path topologies in 2D, 3D, 4D and 5D deviatoric stress or strain spaces. Monte Carlo simulations are performed for  $3 \cdot 10^6$  random 2D history paths, in addition to a few selected paths to try to cover all possible path topologies. All convex hull methods are applied to each of these simulated paths, to evaluate and compare the  $\lambda$  predictions.

Figure 2 compares the  $\lambda$  ratios estimated from the MPH and MPHCC methods, for the  $3 \cdot 10^6$  Monte Carlo simulations. The point  $(\lambda_{MPH}, \lambda_{MPHCC}) = (1, 1)$  in the graph denotes a proportional path, while the point  $(\sqrt{2}, \sqrt{2})$  is obtained for rectangular or circular paths. The “belly” in the graph under the straight line  $\lambda_{MPHCC} = \lambda_{MPH}$  shows that the MPHCC tends to underestimate  $\lambda$  when compared to the MPH, as expected. However, the points located in this “belly” are quite rare: for 2D paths, in average,  $\lambda_{MPHCC}$  is about 98% of  $\lambda_{MPH}$ , with a standard deviation of only 2%. And, even for the rare paths where the  $(\lambda_{MPH}, \lambda_{MPHCC})$  points are located in such “belly,”  $\lambda_{MPHCC}$  never underestimates  $\lambda_{MPH}$  by more than 10%. In addition, the MPHLC and MPHCC usually give almost identical results, with  $\lambda_{MPHLC}$  being in average about 99.85% of  $\lambda_{MPHCC}$ , with a standard deviation of only 0.9% for these  $3 \cdot 10^6$  simulations.

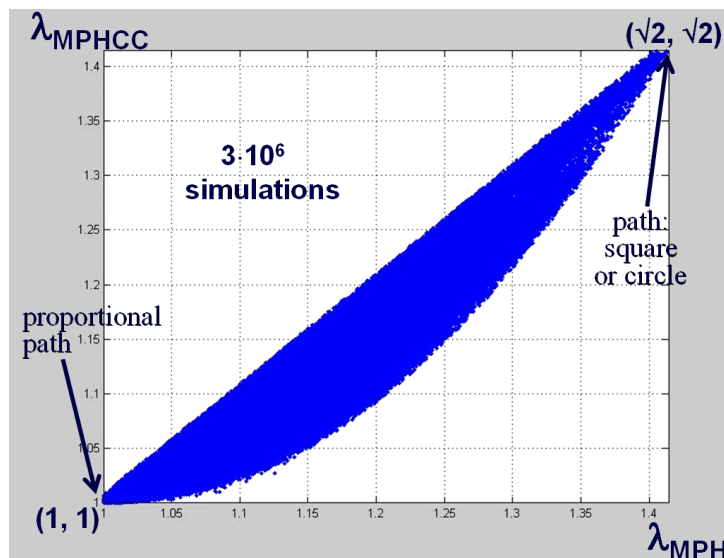


Fig. 2: Comparison between the  $\lambda$  ratios predicted by the MPH and MPHCC methods for  $3 \cdot 10^6$  Monte-Carlo simulations with random 2D history paths.

The Monte Carlo simulations are now used to compare the other convex hull methods. Figure 3 shows that the MPH and MVPH have a very good agreement, except for low values of  $\lambda$ . In addition,  $\lambda_{MVPH} \leq \lambda_{MPH}$  and, in average,  $\lambda_{MVPH}$  is about 98.6% of  $\lambda_{MPH}$ , with a standard deviation of only 1.8%. Similar conclusions are found for 3D, 4D and 5D histories.

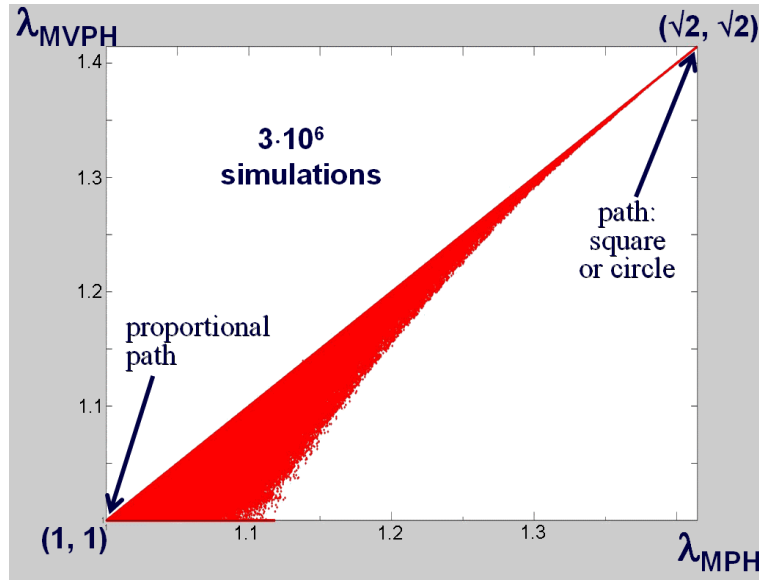


Fig. 3: Comparison between the  $\lambda$  ratios predicted by the MPH and MVPH methods for  $3 \cdot 10^6$  Monte-Carlo simulations with random 2D history paths.

Figure 4 compares the MPH and MFE methods in 2D. Even though these methods seem coherent in the graph, they can lead to very different  $\lambda$  predictions. It is found that  $\lambda_{MFE} \geq \lambda_{MPH}$  and, in average,  $\lambda_{MPH}$  is about 92.9% of  $\lambda_{MFE}$ , with a standard deviation of 4.3%. Similar conclusions are found for 3D, 4D and 5D histories. Note that the point  $(\lambda_{MPH}, \lambda_{MFE}) = (0.5 + \sqrt{3}/2 \cong 1.366, 2\sqrt{2}/\sqrt{3} \cong 1.633)$  in the graph denotes the (extreme) case of a path with the shape of an equilateral triangle. This significant difference between  $\lambda$  predictions suggests that a path shaped like an equilateral triangle would provide a very good discriminant experiment to compare the adequacy of the MPH and MFE methods for a certain material.

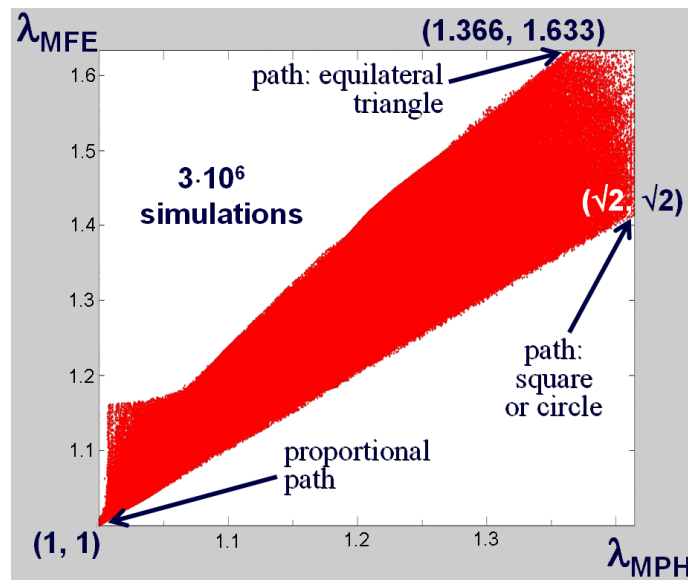


Fig. 4: Comparison between the  $\lambda$  ratios predicted by the MPH and MFE methods for  $3 \cdot 10^6$  Monte-Carlo simulations with random 2D history paths.



Figure 5 compares the MPH and MVE methods in 2D. It is easy to see from the graph that the MVE method can severely (and wrongfully) overestimate  $\lambda$ , in special for low values of  $\lambda_{MPH}$ , associated with almost proportional paths. As discussed before, almost proportional paths can lead to overly elongated ellipses in the MVE method, which can have a small area but an unrealistically large F-norm, leading to  $\lambda_{MVE}$  values larger than 2.0 in some extreme cases. Similar conclusions are found for 3D, 4D and 5D histories.

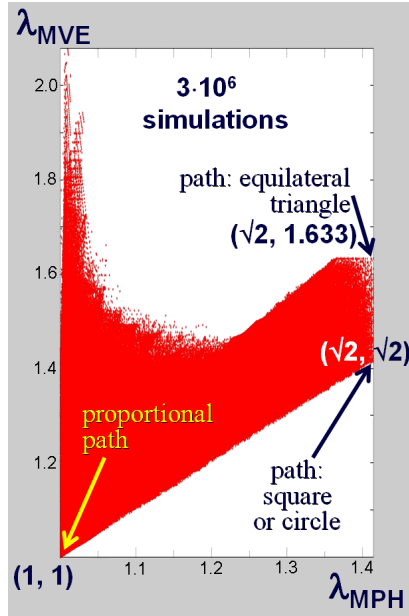


Fig. 5: Comparison between the  $\lambda$  ratios predicted by the MPH and MVE methods for  $3 \cdot 10^6$  Monte-Carlo simulations with random 2D history paths.

Figure 6 compares the MFE and MCE methods in 2D, suggesting that  $\lambda_{MCE}$  overestimates  $\lambda$ , in special for low values of  $\lambda_{MFE}$ , associated with almost proportional paths. For instance, for an almost proportional history defined by a rectangular path with very low aspect ratio, the expected  $\lambda$  would be close to 1.0 (which is the expected value of  $\lambda$  for proportional histories), however the MCE method would circumscribe a circle (instead of an elongated ellipse) to such elongated rectangular path, wrongfully predicting  $\lambda_{MCE} = \sqrt{2}$ . An almost proportional triangular path would also result in this same notable point  $(\lambda_{MFE}, \lambda_{MCE}) = (1, \sqrt{2})$  in the graph, revealing the inadequacy of the MCE method. Similar conclusions are found for 3D, 4D and 5D histories.

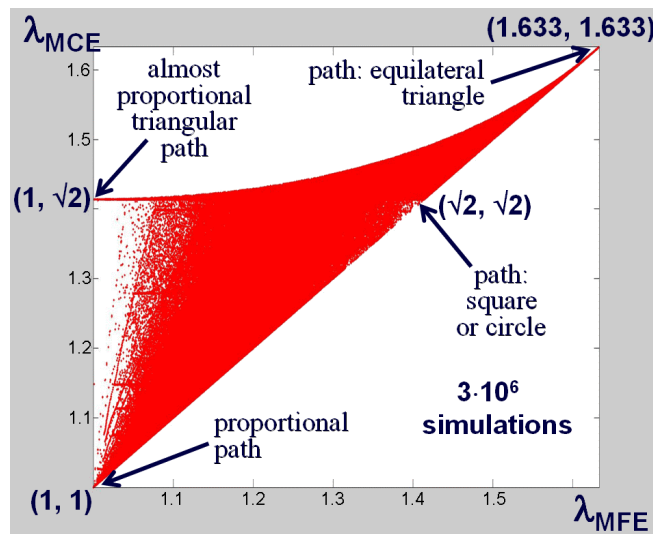


Fig. 6: Comparison between the  $\lambda$  ratios predicted by the MFE and MCE methods for  $3 \cdot 10^6$  Monte-Carlo simulations with random 2D history paths.

Figure 7 compares the MFE and MB methods in 2D. It is easy to see from the graph that the MB method can severely (and wrongfully) underestimate  $\lambda$ , except for almost proportional load histories (where  $\lambda_{MB} \cong \lambda_{MFE} \cong 1.0$ ). Good discriminant experiments to confirm the inadequacy of the MB method could make use of a square or circular path, where  $(\lambda_{MFE}, \lambda_{MB}) = (\sqrt{2}, 1)$ , or a path shaped as an equilateral triangle, where  $(\lambda_{MFE}, \lambda_{MB}) = (2\sqrt{2}/\sqrt{3} \cong 1.633, 2/\sqrt{3} \cong 1.155)$ , see Fig. 7. Both cases would result in  $\lambda_{MFE}/\lambda_{MB} = \sqrt{2}$ , a 41% difference that could be easily verified experimentally. Similar conclusions are found for 3D, 4D and 5D histories.

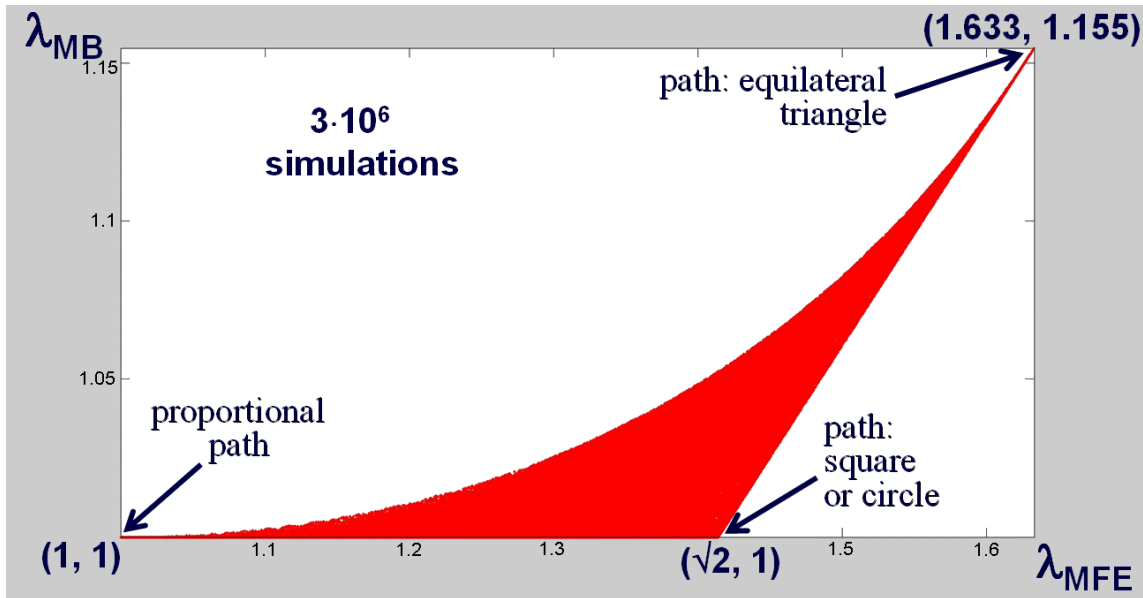


Fig. 7: Comparison between the  $\lambda$  ratios predicted by the MFE and MB methods for  $3 \cdot 10^6$  Monte-Carlo simulations with random 2D history paths.

## 8. Conclusions

In this work, all convex hull methods from the literature were reviewed and compared, and new methods were proposed. The conclusions from the comparisons are:

1. the prismatic hull methods MPHLC and MPHCC are very similar to the MPH and MVPH methods, but with a much simpler search algorithm for 3D to 5D histories;
2. the only recommended ellipsoid hull is the Minimum F-norm Ellipsoid (MFE), which results in similar (but not equal)  $\lambda$  predictions when compared to the prismatic hull methods; and
3. the Minimum Circumscribed Ellipsoid (MCE), Minimum Volume Ellipsoid (MVE), and Minimum Ball (MB) methods may result in very poor predictions of the stress or strain amplitudes.

In summary, the Minimum F-norm Ellipsoid and all four Maximum Prismatic Hull (MPH) models are efficient to predict equivalent amplitudes in NP histories.

## References

- [1] Dang Van, K., Papadopoulos, I.V., High-Cycle Metal Fatigue. Springer 1999.
- [2] Freitas, M., Li, B., Santos, J.L.T., Multiaxial Fatigue and Deformation: Testing and Prediction, ASTM STP 1387, 2000.
- [3] Gonçalves, C.A., Araújo, J.A., Mamiya, E.N., Multiaxial fatigue: a stress based criterion for hard metals, International Journal of Fatigue v.27, pp.177-187, 2005.
- [4] Zouain, N., Mamiya, E.N., Comes, F., Using enclosing ellipsoids in multiaxial fatigue strength criteria, European Journal of Mechanics - A, Solids, v.25, pp. 51-71, 2006.
- [5] Mamiya, E.N., Araújo, J.A., Castro, F.C., Prismatic hull: A new measure of shear stress amplitude in multiaxial high cycle fatigue, International Journal of Fatigue, v.31, pp.1144-1153, 2009.
- [6] Papadopoulos, I.V., Davoli, P., Gorla, C., Filippini, M., Bernasconi, A., "A comparative study of multiaxial high-cycle fatigue criteria for metals", Int. Journal of Fatigue v.19, pp.219–235, 1997.

- [7] Bernasconi, A., Efficient algorithms for calculation of shear stress amplitude and amplitude of the second invariant of the stress deviator in fatigue criteria applications, *International Journal of Fatigue*, v.24, n.6, pp.649-657, 2002.
- [8] Deperrois, A., Sur le calcul des limites d'endurance des aciers. Thèse de Doctorat. Ecole Polytechnique, Paris, 1991.
- [9] Ballard, P., Dang Van, K., Deperrois, A., Papadopoulos, I.V., High Cycle Fatigue and a Finite Element Analysis, *Fatigue Fract. Engng. Mater. Struct* v.18, n.3, pp.397-411, 1995.